Inorganic Chemistry

pubs.acs.org/IC Article

Controllable Syntheses, Crystal Structure Evolution, and Photoluminescence of Polymorphic Zirconium Oxyfluorides

Chen Li, Ting Wen, Ke Liu, Dequan Jiang, Zimin Jiang, and Yonggang Wang*

HPSTAR 1248-2021

Cite This: *Inorg. Chem.* 2021, 60, 14382−14389 Read Online

ACCESS | Metrics & More | Article Recommendations | Supporting Information

ABSTRACT: Precise synthesis of polymorphic phases with similar components but distinct crystal structures is one of the key problems in inorganic chemistry. In this work, we report a fluorination method adopting ZrO_2 as the starting material and NH_4F as the fluoridation agent that can afford multiphases in the Zr−O−F system, including $Zr_7O_9F_{10}$, $Zr_3O_2F_8$, $ZrO_{0.46}F_{3.08}$, $ZrO_{0.33}F_{3.33}$, β-ZrF_4, $NH_4Zr_2F_9$, and NH_4ZrF_5. A preliminary phase formation diagram was established as a function of the fluorination temperature (T), reaction time (t), and F/Zr ratio after systematic optimization of the preparation conditions. Among the as-obtained phases, the detailed crystal structures of $Zr_7O_9F_{10}$ and $ZrO_{0.33}F_{3.33}$ were refined based on the powder X-ray diffraction patterns. As the F/O ratio increases, the crystal structures of Zr−O−F phases transform gradually from an anion-deficient α-UO_3-related structure of $Zr_7O_9F_{10}$ to an anion-excess ReO_3-related structure of $ZrO_{0.33}F_{3.33}$. At last, we also prepared Ti-doped ZrO_2, $Zr_7O_9F_{10}$, $ZrO_{0.46}F_{3.08}$, and $ZrO_{0.33}F_{3.33}$ to study the host-lattice-dependent photoluminescence properties of zirconium oxyfluorides. The four materials show distinct photoluminescence in the UV and visible regions due to different local coordination environments of Zr/Ti. This work demonstrates the low-temperature fluorination method as an efficient route to phase-selective polymorphic metal oxyfluorides, which can be employed in further structure−property relationship studies.

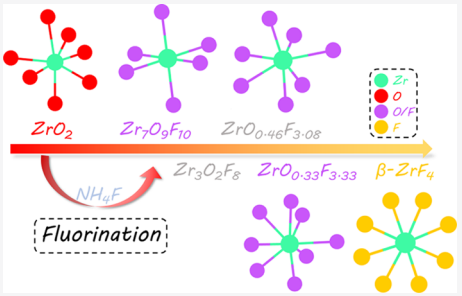

1. INTRODUCTION

Mixed-anion compounds, represented by oxyhalides, take on great research value in the fields of magnetism, photocatalysis, electrodes, fluorescence, and nonlinear optics due to their diversity in structural and physical properties.[1−6] For a given metal cation, there always exist several oxyhalide phases with distinct structures and different stoichiometries. Thus, the precise synthesis of polymorphic phases with similar components but distinct crystal structures has been the core problem in inorganic chemistry. Polymorphic mixed-anion materials can provide an excellent platform for the comparative study of the structure−property relationship. For example, bismuth oxyhalides $Bi_xO_yM_z$ (M = Cl, Br, and I) with different components and crystal structures exhibit distinct optical absorption behaviors in the visible region and diverse photocatalytic performances.[7−11] Considering the extremely variable local structure and multifunctionality of metal oxyhalides, it is of great significance to explore facile and efficient preparation routes toward polymorphic metal oxyhalides.

Among the various oxyhalides, the syntheses of metal oxyfluorides are of particular difficulty because of the toxicity of fluorine and fluorochemicals. In the past, they have been generally synthesized by gas fluorination, the hydrothermal method, and the direct solid-state method under protecting conditions.[12−14] The traditional solid-state method adopts stoichiometric oxide and fluoride as the raw materials, and they react in a vacuum ampoule to produce the target oxyfluoride. For example, Papiernik and Frit reported the synthesis of $ZrO_{0.67}F_{2.67}$ by heating zirconia and zirconium fluoride within a sealed Pt tube.[14] However, such a process is expensive and complicated and can only produce thermodynamic-stable phases. The exploration of new and efficient preparation methods of oxyfluorides has attracted much attention in the past decades. Low-temperature fluorination using metal oxides as raw materials is one of the typical methods. NH_4HF_2, polyvinylidene fluoride (PVDF), and polytetrafluoroethylene (PTFE) are commonly used as the fluoridation agents in this method.[15−20] Flynn et al. reported the fluoridation of HfO_2 using PVDF, PTFE, and NH_4HF_2 as solid-state fluoridation agents, which afforded either single-phase or multiple-phase hafnium oxyfluorides, respectively.[15] Hirai et al. used PTFE as the fluorinating agent to prepare $Nb_5O_{12}F$, Nb_3O_7F, Ta_3O_7F, TaO_2F, and $Mo_4O_{11.2}F_{0.8}$ successfully from Nb_2O_5, Ta_2O_5, and MoO_3.[17] In these reaction processes, the fluoridation agents are considered to decompose into F-containing gases, react with the oxides, and meanwhile act as protective atmospheres for the products. Nevertheless, the low-temperature fluorina-

Received: July 19, 2021
Published: September 1, 2021

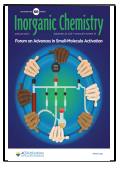

https://doi.org/10.1021/acs.inorgchem.1c02176
Inorg. Chem. 2021, 60, 14382−14389

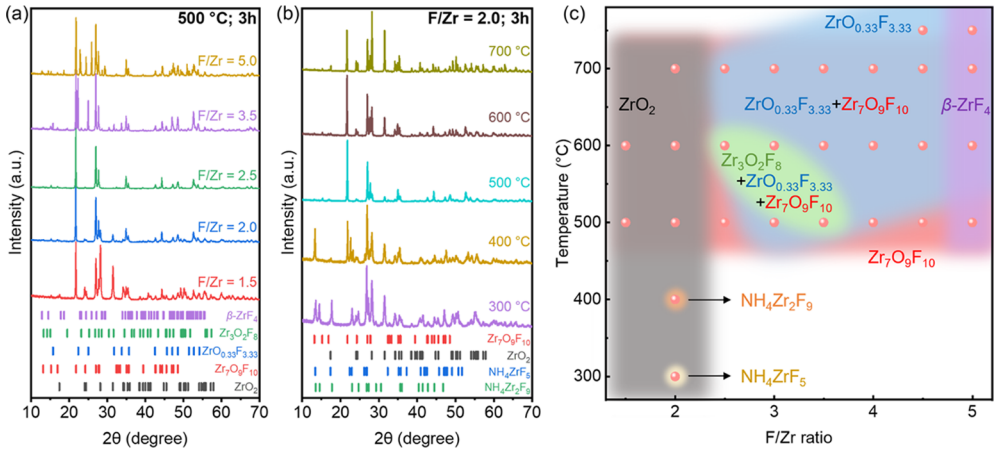

Figure 1. (a) Powder XRD patterns of the products with various F/Zr ratios; (b) powder XRD patterns of the products with different temperatures; and (c) phase formation diagram of the fluorination reaction from ZrO_2 at various F/Zr ratios and different temperatures for 3 h (pink balls: specific reaction conditions).

tion method has only been reported in limited several oxyfluoride systems until now. Further exploration and precise fluorination syntheses are needed for more functional metal oxyfluorides.

Zirconium oxyfluorides have been reported to have multiphases with components ranging from ZrO_2 to ZrF_4 and diverse structure types due to the flexible coordination habits of Zr^{4+}, which were synthesized in sealed evacuated tubes.[21−23] In addition to the above preparation methods, Kolditz and Feltz had synthesized zirconium oxyfluorides by thermal decomposition of zirconium tetrafluoride hydrates and hydroxides;[24] Plitzko and Meyer used metal powder and NH_4HF_2/NH_4F as raw materials in the preparation process.[25,26] Besides, the syntheses of ammonium fluorozirconates using ZrF_4 and NH_4F in solvents had also been studied.[27,28] Zirconium oxyfluorides have the potential to find application as O^{2-}/F^- ionic conductors and candidates for host lattices for trivalent or tetravalent metal-doped fluorescent materials. Surprisingly, only three zirconium oxyfluorides have become available with the structural information in the ICSD database until now, that is, ZrO_xF_{4-x} with $x = 0.67$ and 1.29, respectively ($x = 0.67$ corresponds to two cubic crystal structures).[14,21,29] In the process of preparing zirconium oxyfluorides, a variety of thermodynamic metastable phases appear. It is difficult to obtain the respective pure phases, which hinders the collection of crystal structure data.[30−32] Herein, we report a convenient fluorination method starting from ZrO_2 and using NH_4F as the fluorination agent, which can produce a series of polymorphic zirconium oxyfluorides in a controllable manner. A phase formation diagram was established as a function of fluorination temperature (T), reaction time (t), and the F/Zr ratio. Moreover, these local-structure-distinct zirconium oxyfluorides were employed as host lattices for Ti doping to verify the structure−property relationship.

2. EXPERIMENTAL SECTION

2.1. Syntheses of Zirconium Oxyfluorides. ZrO_2 (Aladdin, 99.99%, removed Hf or HfO_2) and NH_4F (Aladdin, 99.99%) with different stoichiometric amounts were ground thoroughly in an agate mortar and then placed in alumina crucibles. After crucibles were covered, they were put into the muffle furnace to heat for 2−4 h at different temperatures ranging from 300 to 800 °C at a heating rate of 5 °C/min. Meanwhile, the heating procedure was repeated with a dry Ar flow at 20 mL/min under various conditions of the reaction at 500−750 °C for 2/3 h.

2.2. Syntheses of Ti-Doped Zirconium Oxyfluorides. First, 0.1% Ti-doped ZrO_2 was prefabricated as the raw material for the further fluoridation reaction. ZrO_2 and TiO_2 (Aladdin, 99.99%) with the molar ratio of 1:0.001 were fully ground and calcined at 1500 °C for 5 h in an air atmosphere. Then, Ti-doped ZrO_2 was mixed with NH_4F, and the reaction conditions were similar to that with the undoped samples.

2.3. Characterization. Powder X-ray diffraction (XRD) patterns at room temperature were obtained using a PANalytical Empyrean diffractometer on Cu Kα radiation under three setting parameters, that is, the 2θ angle ranges of 5−70, 5−80, and 5−120° with the angle steps of 0.01313, 0.01313, and 0.00656°, respectively. Rietveld refinements and LeBail fittings were performed based on the powder XRD patterns of the as-obtained products using Fullprof Suite software. Crystal structures were visualized with software VESTA. Raman spectra were recorded at room temperature using a Renishaw inVia reflex micro-Raman spectroscope with a 532 nm laser. The room-temperature excitation and emission spectra were measured on a Hitachi F-4600 spectrophotometer. The photoluminescence (PL) and afterglow properties were tested at 254 nm using a UV lamp.

3. RESULTS AND DISCUSSION

3.1. Phase-Selective Syntheses. Fluorination of ZrO_2 using NH_4F as the fluorination agent affords multiphase zirconium oxyfluorides according to the following equation

$$ZrO_2 + NH_4F \rightarrow ZrO_xF_{4-2x} + NH_3\uparrow + H_2O\uparrow \quad (1)$$

Three reaction parameters are found to be crucial for the final products: reaction temperature (T), fluorination time (t), and the F/Zr ratio. First of all, a suitable reaction time of $t = 3$ h was established after some attempts and fixed in all the subsequent fluorination reactions. Then, the fluorination temperature was fixed at $T = 500$ °C to estimate the impact of the F/Zr ratio (NH_4F/ZrO_2) on the resulting products. Figure 1a shows the results of the tests with the F/Zr ratio ranging from 1.5 to 5.0. Under these conditions, the main product was $Zr_7O_9F_{10}$, but the secondary phase shows a regular change with the increasing F/Zr ratio. With the F/Zr ratio below 2.5, unreacted ZrO_2 was found in the products, and a F/Zr ratio of 2.5 was found to be the most suitable condition for the formation of $Zr_7O_9F_{10}$ as a pure phase. As the F/Zr ratio continues to increase, ZrO_2 in the product disappears, and other oxyfluorides appear in the reaction products. For

https://doi.org/10.1021/acs.inorgchem.1c02176
Inorg. Chem. 2021, 60, 14382−14389

example, when F/Zr = 3.5, the product is mixed phases of multiple oxyfluorides, including $Zr_7O_9F_{10}$, $Zr_3O_2F_8$, and $ZrO_{0.33}F_{3.33}$ (Zr_3OF_{10}), and when F/Zr = 5.0, the products are $Zr_7O_9F_{10}$ and β-ZrF_4 (monoclinic phase). It can be seen that as the amount of NH_4F in the reactant increases, the proportion of the F element contained in the phase of the product also increases.

Then, the effect of the reaction temperature (T) on the formation of zirconium oxyfluorides was studied in the fluorination process. In this case, the F/Zr ratio is fixed at 2.0, and the fluorination time (t) is fixed at 3 h. The relationship between the phase formation determined by powder XRD and t was obtained and is shown in Figure 1b. At the lowest T = 300 °C, some unreacted ZrO_2 remains in the product, and the reactant is slightly fluorinated to produce $NH_4Zr_2F_9$. When T increases to 400 °C, NH_4ZrF_5 is produced, and the first oxyfluoride member $Zr_7O_9F_{10}$ appears in the product simultaneously. Above 500 °C, the ammonium fluorozirconate compounds disappear, and the products contain two main phases, $Zr_7O_9F_{10}$ and ZrO_2. As the temperature continues to rise, the content of ZrO_2 begins to increase. This is because when the temperature is high, the generated oxyfluorides will be hydrolyzed with the water vapor in the product or in air to form oxides. The decomposition of zirconium oxyfluorides by water vapor may be described as

$$ZrO_xF_{4-2x} + H_2O \rightarrow ZrO_2 + HF \quad (2)$$

Notably, there was no fluoride ZrF_4 in all groups, which was caused by the insufficient amount of the fluorinating agent NH_4F with the F/Zr ratio = 2.0. Laptash and Polyshchuk had reported the reaction mechanism of Fe_2O_3 and NH_4HF_2.[33] The two reactants generate $(NH_4)_3FeF_6$ at 200 °C, which thermally decomposes to NH_4FeF_4 at 280 °C and finally to FeF_3 at 410 °C. This phenomenon is similar to the fluorination results as a function of fluorination time (t) in our experiment.

Figure 1c displays the phase formation diagram of the fluorination reaction from ZrO_2 at various F/Zr ratios and different temperatures for 3 h. One can conclude that the unreacted raw material ZrO_2 always appears in the product when the F/Zr ratio is less than 2, and the postfluorinated β-ZrF_4 appears when the F/Zr ratio is more than 4.5. When the reaction temperature is below 400 °C, two ammonium fluorozirconate phases appear in the product, and when the reaction temperature continues to rise, the main phase of the product gradually changes to multiphases of zirconium oxyfluorides. In the diagram, it is also obvious that the $Zr_7O_9F_{10}$ phase exists in a wide range of T values and F/Zr ratios, while the phase formation region of $Zr_3O_2F_8$ is narrower, and the phase fraction in the product is relatively low. It is worth mentioning that $ZrO_{0.46}F_{3.08}$ can also be prepared when reducing the reaction time to 2 h. In the synthesis experiments, phase-pure zirconium oxyfluorides $Zr_7O_9F_{10}$ and $ZrO_{0.33}F_{3.33}$ have been synthesized by low-temperature fluorination under reaction conditions of 500 °C with F/Zr = 2.5 for 3 h and 750 °C with F/Zr = 4.5 for 3 h, respectively.

Considering the influence of water vapor generated during the reaction, the samples were synthesized again under the same reaction conditions as possible (reaction time and temperature) under a dry Ar flow. The powder XRD patterns of the obtained products are shown in Figure S1. It can be seen that all oxyfluorides and fluorides obtained by the reaction in the air atmosphere can be prepared. The specific product composition is not exactly the same, which again shows that the water content does affect the reaction process. However, the phase formation rules under different reaction atmospheres are similar. β-ZrF_4 is formed with a high F/Zr ratio; $Zr_7O_9F_{10}$ is obtained under a wide range of conditions; and it is easier to prepare pure $ZrO_{0.33}F_{3.33}$ at higher temperatures. Such rules are very helpful for the syntheses of system phases.

3.2. Crystal Structure Refinements. $Zr_7O_9F_{10}$ and $ZrO_{0.33}F_{3.33}$ are white powders, indicating that they are both wide-band-gap insulators. Figure 2 shows the structure

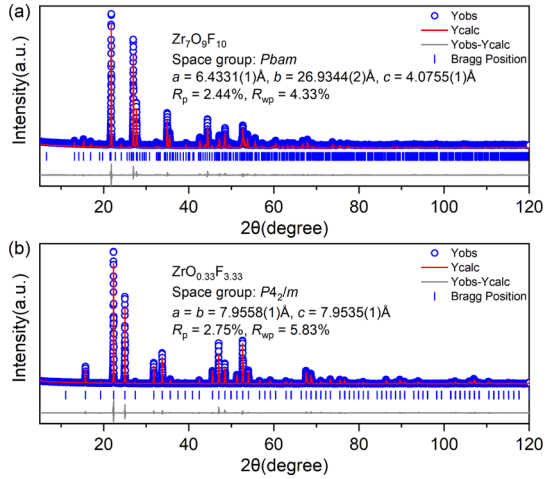

Figure 2. Rietveld refinements of powder XRD profiles of (a) $Zr_7O_9F_{10}$ and (b) $ZrO_{0.33}F_{3.33}$.

refinement results of $Zr_7O_9F_{10}$ and $ZrO_{0.33}F_{3.33}$ based on the powder XRD patterns. Crystallographic details are summarized in Table S1. $Zr_7O_9F_{10}$ crystallizes in the orthorhombic space group *Pbam*, and the refined unit cell parameters are a = 6.4331(1) Å, b = 26.9344(2) Å, and c = 4.0755(1) Å with R_p = 2.44% and R_{wp} = 4.33%. The as-obtained unit cell parameters are consistent with those prepared by the direct solid-state method reported by Holmberg [a = 6.443(1) Å, b = 26.851(1) Å, and c = 4.071(1) Å].[29] In the lattice of $Zr_7O_9F_{10}$, F and O occupy the same site with different occupancies, as shown in Table S2. The structure of $ZrO_{0.33}F_{3.33}$ was reported by Papiernik and Frit to crystallize in space group $P4/mbm$ with lattice parameters a = b = 7.946(1) Å and c = 3.970(1) Å on a single crystal study.[34] However, the result of Rietveld refinement of the $ZrO_{0.33}F_{3.33}$ phase synthesized in this work with this structure is not satisfactory, which is reflected in that partial diffraction peaks are not indexed, including 19.3, 37.4, 49.9, 60.4, 69.9, 87.5, 96.1, and 114.0°. While using the structure of tetragonal ZrF_4 (ICSD #35100) as an initial model,[35] all the diffraction peaks can be fitted very well, as shown in Figure S2. In addition, the appearance of wider and more diffuse diffraction peaks with odd hkl reflections [e.g., (111), (311), (511), and (531)] also confirms the integrity of the structure with the $P4_2/m$ space group (Figure S3). Thus, the structure refinement of $ZrO_{0.33}F_{3.33}$ was performed using the structure of tetragonal ZrF_4. $ZrO_{0.33}F_{3.33}$ crystallizes in the tetragonal space group $P4_2/m$ with the unit cell parameters a = b = 7.9558(1) Å and c = 7.9535(1) Å with R_p = 2.75% and R_{wp} = 5.83%. The refined atomic positions and occupancy rates are shown in Table S3.

The crystal structure of $Zr_7O_9F_{10}$ can be considered as an anion-deficient α-UO_3-related structure.[39] Zr atoms are located

https://doi.org/10.1021/acs.inorgchem.1c02176
Inorg. Chem. 2021, 60, 14382−14389

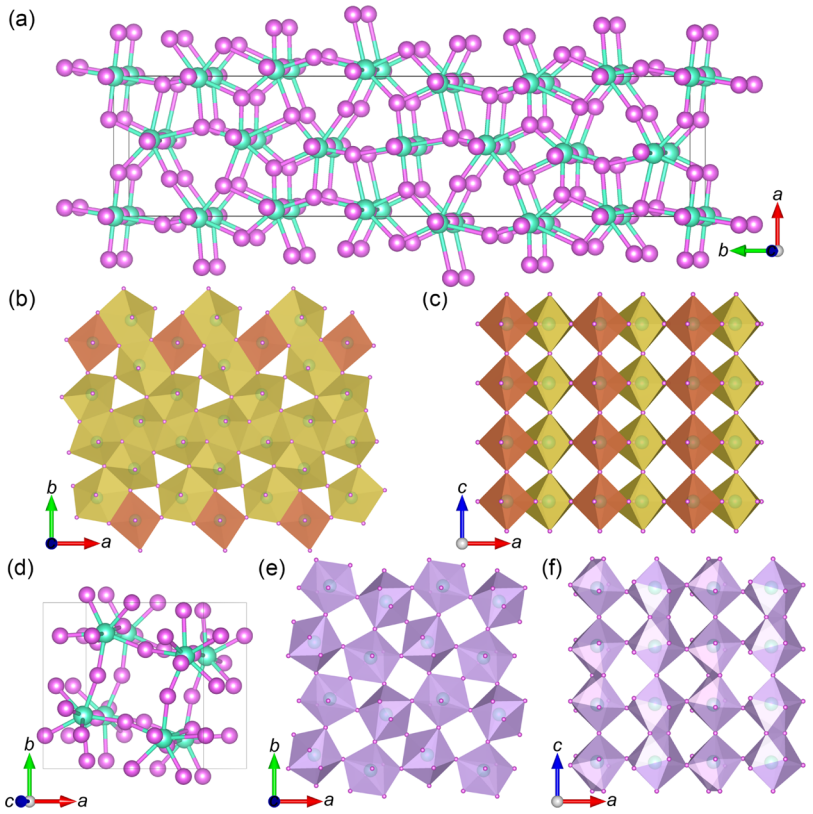

Figure 3. Crystal structures of $Zr_7O_9F_{10}$ and $ZrO_{0.33}F_{3.33}$. (a) Unit cell of $Zr_7O_9F_{10}$; (b) coordination polyhedra of $Zr_7O_9F_{10}$ in the (001) plane; (c) coordination polyhedra of $Zr_7O_9F_{10}$ in the $(0\bar{1}0)$ plane; (d) unit cell of $ZrO_{0.33}F_{3.33}$; (e) coordination polyhedra in the (001) plane; and (f) coordination polyhedra of $ZrO_{0.33}F_{3.33}$ in the $(0\bar{1}0)$ plane (green balls: Zr and purple balls: F/O).

in the sixfold or sevenfold coordinated polyhedra, that is, slightly distorted $Zr(O/F)_6$ octahedra and $Zr(O/F)_7$ pentagonal bipyramids, respectively. As shown in Figure 3a–c, in the (001) plane, the coordination polyhedra are connected by edges and corners; while in the *c*-axis direction, the coordination polyhedra are connected by corners to form a three-dimensional structure. The structure of $ZrO_{0.33}F_{3.33}$ can be described based on the known structure of tetragonal ZrF_4. The F/O sites in the $ZrO_{0.33}F_{3.33}$ lattice are not fully occupied, indicating that it is a disordered structure. Similar to that in tetragonal ZrF_4, Zr atoms are located in dodecahedral sites with the surrounding eight F/O atoms. The dodecahedra share the edges and corners in the (001) plane and share the corners in the $(0\bar{1}0)$ plane to form a three-dimensional structure. Thus, the crystal structure of $ZrO_{0.33}F_{3.33}$ can be described as an anion-excess ReO_3-related structure, as shown in Figure 3d–f.

3.3. Structure Evolution of the Zr–O–F System. The polymorphic phases presented in the Zr–O–F system are shown in Table 1. In the NH_4F-based fluorination processes, four oxyfluoride phases are available: $Zr_7O_9F_{10}$, $Zr_3O_2F_8$, $ZrO_{0.46}F_{3.08}$, and $ZrO_{0.33}F_{3.33}$, together with fluoride β-ZrF_4. Among them, $Zr_7O_9F_{10}$ and $ZrO_{0.33}F_{3.33}$ can be prepared as pure phases, while $Zr_3O_2F_8$, $ZrO_{0.46}F_{3.08}$, and β-ZrF_4 appear as mixed phases. Nevertheless, LeBail fitting analyses are still feasible based on the powder XRD patterns using the initial parameters from the known hexagonal $Zr_3O_2F_8$ (PDF #38-0704), orthorhombic $ZrO_{0.46}F_{3.08}$ (PDF #20-1472), and monoclinic ZrF_4 (ICSD #165289) (as shown in Figure S4).

The crystal structure evolution of zirconium oxyfluorides is highly related with those of the end members: ZrO_2 and ZrF_4. First of all, the starting material ZrO_2 used in the experiment is a monoclinic phase, which is reported to transform to a tetragonal phase at 1100 °C and to a cubic phase above 2200 °C.[40] In monoclinic ZrO_2, Zr coordinates with the surrounding O atoms to form a ZrO_7 single-cap triangular prism, which connects with edges and corners to form a three-dimensional framework. There exist three crystalline α, β, and γ phases and one amorphous form for ZrF_4.[41] This work involves two phases: a monoclinic phase β-ZrF_4 and a tetragonal phase α-

Table 1. Polymorphic Phases Presented in the Zr–O–F System (CN: Coordination Number)

phase	F/Zr ratio	CN	space group	cell parameters	notes
m-ZrO_2	0.00	7	$P2_1/c$	a = 5.145 Å, b = 5.210 Å, c = 5.312 Å, β = 99.23°	ref 36
$Zr_7O_9F_{10}$	1.42	6, 7	*Pbam*	a = 6.433 Å, b = 26.93 Å, c = 4.076 Å	this work
$Zr_7O_9F_{10}$	1.42	6, 7	*Pbam*	a = 6.443 Å, b = 26.85 Å, c = 4.071 Å	ref 29
$Zr_3O_2F_8$	2.67		$P6_3mc$	a = 7.664 Å, c = 12.48 Å	this work
$Zr_3O_2F_8$	2.67		$P6_3mc$	a = 7.671 Å, c = 12.49 Å	ref 37
$ZrO_{0.67}F_{2.67}$	2.67	6, 7	$Pm\bar{3}m$	a = 3.997 Å	ref 14
$ZrO_{0.46}F_{3.08}$	3.08		*Pmmm*	a = 11.91 Å, b = 7.849 Å, c = 4.015 Å	this work
$ZrO_{0.33}F_{3.33}$	3.33	8	$P4_2/m$	a = 7.956 Å, c = 7.954 Å	this work
$ZrO_{0.33}F_{3.33}$	3.33	7, 8	$P4/mbm$	a = 7.946 Å, c = 3.970 Å	ref 34
α-ZrF_4	4.00	8	$P4_2/m$	a = 7.896 Å, c = 7.724 Å	ref 35
β-ZrF_4	4.00	8	$I2/c$	a = 9.547 Å, b = 9.936 Å, c = 7.699 Å, β = 94.53°	this work
β-ZrF_4	4.00	8	$I2/c$	a = 9.570 Å, b = 9.930 Å, c = 7.730 Å, β = 94.28°	ref 38

https://doi.org/10.1021/acs.inorgchem.1c02176
Inorg. Chem. 2021, 60, 14382–14389

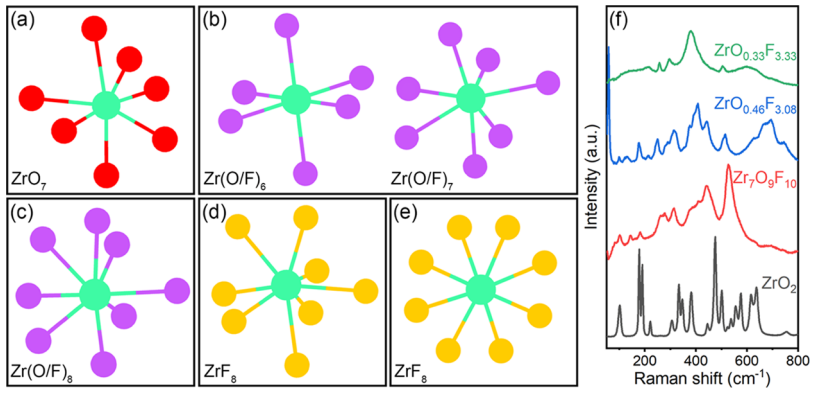

Figure 4. Schematic diagram of different coordination forms of Zr in (a) *m*-ZrO_2, (b) $Zr_7O_9F_{10}$, (c) $ZrO_{0.33}F_{3.33}$, (d) α-ZrF_4, and (e) β-ZrF_4 and (f) Raman spectra of different phases in the Zr−O−F system under 532 nm radiation.

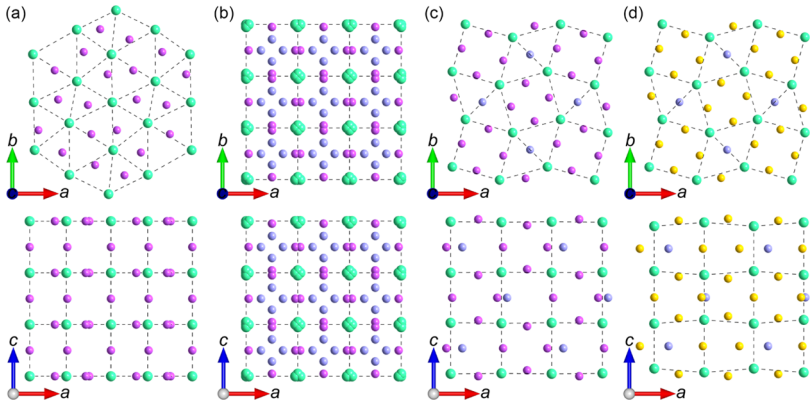

Figure 5. Networks of Zr in different phases: (a) orthorhombic $Zr_7O_9F_{10}$; (b) cubic $ZrO_{0.67}F_{2.67}$; (c) tetragonal $ZrO_{0.33}F_{3.33}$; and (d) tetragonal ZrF_4 (green balls: Zr; purple balls: F/O; yellow balls: F; and pale blue balls: the corresponding atoms occupying the excess anion sites of cubic ReO_3).

ZrF_4. Monoclinic β-ZrF_4 is a stable phase that exists at room temperature, and tetragonal α-ZrF_4 is a metastable phase that exists at high temperature and can be stabilized to room temperature by quenching. In our experiments, only the monoclinic phase β-ZrF_4 is found in the products, but it is reasonable to infer that under the dynamic fluorination conditions, there should be an α-ZrF_4 phase at high temperature due to the great structural similarity between α-ZrF_4 and polymorphic zirconium oxyfluorides. In practice, the crystal structure of tetragonal ZrF_4 was referenced when performing structure refinement of $ZrO_{0.33}F_{3.33}$. In the Zr−O−F system, the coordination forms of Zr are varied, such as the sevenfold coordinated Zr in *m*-ZrO_2, the sixfold or sevenfold coordinated Zr in $Zr_7O_9F_{10}$, and the eightfold coordinated Zr in $ZrO_{0.33}F_{3.33}$ and α-ZrF_4 (Figure 4a−e).

Raman spectra were measured to study the local structures of selected polymorphic zirconium oxyfluorides (Figure 4f). The Raman peaks of the starting material ZrO_2 are intense and easier to distinguish. The peaks appearing at 102, 190, 305, 348, 476, 556, and 637 cm^{-1} correspond to the A_g symmetry modes, while the peaks at 222, 334, 381, 500, 534, and 615 cm^{-1} correspond to the B_g modes.[42] For $Zr_7O_9F_{10}$, complex Raman bands instead of sharp peaks are observed at approximately 83, 102, 145, 181, 261, 277, 313, 375, 410, 441, and 526 cm^{-1}, probably due to the coexistence of $Zr(O/F)_6$ octahedra and $Zr(O/F)_7$ pentagonal bipyramids. Since the $ZrO_{0.46}F_{3.08}$ sample contains a small amount of $Zr_7O_9F_{10}$, some Raman bands of the obtained Raman spectra are similar to that of $Zr_7O_9F_{10}$. The difference is that a strong peak appears at 59 cm^{-1} and Raman bands appear at 627, 665, 693, and 735 cm^{-1}. From the Raman spectra of $ZrO_{0.33}F_{3.33}$, five weak Raman bands at 213, 258, 294, 503, and 600 cm^{-1} and a strong band at 380 cm^{-1} can be distinguished. With reference to the molecular ZrF_8 dodecahedron,[43] the Raman bands at 258, 380, and 503 cm^{-1} can be assigned to the B_1 modes, B_2 modes, and A_1 modes, respectively. In brief, with the F-replacement of O^{2-} in zirconium oxyfluorides, the O/F disorder comes into being, and thus, the Raman peaks gradually broaden into Raman bands. Due to the different coordination forms of Zr and the distortion of the coordination polyhedra, the Raman spectra of different oxyfluoride phases are quite distinct.

The networks of Zr in the Zr−O−F system show an interesting evolution from $Zr_7O_9F_{10}$ to ZrF_4 (Figure 5). Orthorhombic $Zr_7O_9F_{10}$ is the first oxyfluoride member close to the ZrO_2 end, which adopts an anion-deficient α-UO_3-related structure. The second oxyfluoride member, cubic $ZrO_{0.67}F_{2.67}$, is available in the ICSD database (#29353).[14] Zr^{4+} cations are arranged disorderly in the lattice with a framework deriving from the cubic closest-packed structure. The overall crystal structure of $ZrO_{0.67}F_{2.67}$ can be actually described as an anion-excess ReO_3-related structure (Figure 5b), in which the F^-/O^{2-} anions occupy the excess sites beyond those in the ReO_3 structure. Although tetragonal $ZrO_{0.33}F_{3.33}$ also has an anion-excess ReO_3-related structure, the lower symmetry of the Zr network leads to a $3^2.4.3.4$ (001) cationic plane net deformed from the 4^4 square net. As the distance between Zr

https://doi.org/10.1021/acs.inorgchem.1c02176
Inorg. Chem. 2021, 60, 14382−14389

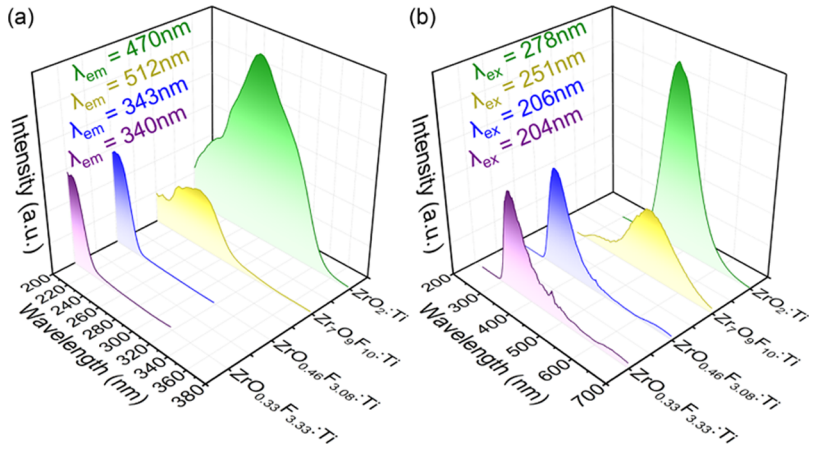

Figure 6. (a) Excitation and (b) emission spectra of different Ti-doped zirconium oxyfluorides (the intensity of the yellow line is multiplied 5 times).

atoms is further shortened, the 4^4 square net is gradually distorted in the $(0\bar{1}0)$ plane, indicating that the symmetry of the lattice increases first and decreases later. In brief, as the proportion of the F element in the phase increases, the crystal structure changes from an anion-deficient α-UO_3-related structure to the anion-excess ReO_3-related structure.

3.4. Photoluminescence Spectra of Ti-Doped Zirconium Oxyfluorides. Traditional and afterglow Ti-doped ZrO_2 materials are potential candidates for specific applications in which other aluminate phosphors cannot be applied.[44−47] According to the experimental results previously reported,[45,46] 0.1% was determined as the best doping concentration of Ti. It is well-known that the PL properties of transition metal or rare earth cations are highly dependent on the coordination environment of the doping sites. Since Zr^{4+} has a variety of coordination forms in the polymorphic zirconium oxyfluorides (coordination number from 6 to 8 and distortion of the polyhedra), they provide an ideal platform for studying the local-structure-dependent PL properties of Ti-doped zirconium oxyfluorides. Therefore, four phases with 0.1% Ti doping were synthesized, namely, ZrO_2:Ti, $Zr_7O_9F_{10}$:Ti, $ZrO_{0.46}F_{3.08}$:Ti, and $ZrO_{0.33}F_{3.33}$:Ti (as shown in Figure S5).

Considering that the content of doped Ti is very low, it is difficult to detect the influence of possible impurities in the product on the luminescence properties of oxyfluorides, such as the most likely impurity of TiF_3−ZrF_4 solid solutions. Fortunately, the synthesis and properties of such compounds have been previously reported.[48,49] Through the characterization of UV−vis absorption spectroscopy, it is found that these phases are all semiconductors with narrow band gaps, which are unlikely to emit visible or UV light under the excitation of ultraviolet wavelength. For example, the band gap (E_g) values of $TiZrF_{6.5}$ and $TiZrF_7$ are 0.93 and 1.04 eV, respectively. Thus, the interference of such possible impurities on the luminescence performance of the oxyfluorides can be excluded. Moreover, the Ti element participates in the fluorination process in the zirconia lattice, which can be proved from ZrO_2:Ti with the long-afterglow-emission property of green light. Therefore, we believe that Ti tends to exist in the oxyfluoride lattice after fluorination.

As shown in Figure S6, ZrO_2:Ti has a bright green emission under a 254 nm UV lamp, and it can emit continuously for up to tens of seconds after turning off the light. $Zr_7O_9F_{10}$:Ti emits yellow light under the same excitation, and there is no afterglow PL when the light source is turned off. $ZrO_{0.46}F_{3.08}$:Ti and $ZrO_{0.33}F_{3.33}$:Ti have only faint yellow emission, and also, no afterglow PL is observed. Figure 6 shows the excitation and emission spectra of ZrO_2:Ti and three Ti-doped oxyfluorides. Both ZrO_2:Ti and $Zr_7O_9F_{10}$:Ti emit in the visible light range, with a green emission at 470 nm and a yellow emission at 512 nm, respectively. It is already known that the green emission of ZrO_2:Ti originates from the charge transfer of Ti.[50] After fluorination, the d−d transition of Ti^{3+} may lead to the yellow emission. Surprisingly, the excitation and emission spectra of $ZrO_{0.46}F_{3.08}$:Ti and $ZrO_{0.33}F_{3.33}$:Ti are sufficiently similar, the emission peaks of both are located in the UV range, appearing at 343 and 340 nm. Nevertheless, the excitation spectra indicate that the main excitation peaks of Ti-doped zirconium oxyfluorides gradually show a blue shift from 278 to 204 nm with the increasing F/O ratio. Since the electronegativity of fluorine atoms is larger than that of oxygen atoms, higher energy is required for electronic excitation,[51] which may result in the blue shift of the excitation peaks. Besides, the different emission performance may be caused by different depths of trap levels formed after Ti replaces Zr in various coordination environments.

4. CONCLUSIONS

In summary, a series of zirconium oxyfluorides were prepared by low-temperature fluorination using NH_4F as the fluorinating agent. A phase formation diagram was drawn for the Zr−O−F system as a function of the reaction temperatures and reactant ratios. The results show that the higher the reaction temperature or the higher the F/Zr ratio is, the higher the fluorine fractions in the final phases are. As the proportion of fluorine increases, the crystal structures of the polymorphic zirconium oxyfluorides gradually transform from an anion-deficient α-UO_3-related structure of $Zr_7O_9F_{10}$ into an anion-excess ReO_3-related structure of $ZrO_{0.33}F_{3.33}$. Finally, Ti-doped zirconium oxyfluorides were employed as host lattices to study the local-structure-related PL properties. These results not only demonstrate the low-temperature fluorination method as an efficient route to multiple phases but also provide an in-depth understanding of the phase formation of mixed-anion compounds in dynamic conditions.

https://doi.org/10.1021/acs.inorgchem.1c02176
Inorg. Chem. 2021, 60, 14382−14389

■ ASSOCIATED CONTENT

Supporting Information

The Supporting Information is available free of charge at https://pubs.acs.org/doi/10.1021/acs.inorgchem.1c02176.

LeBail fitting results, powder XRD patterns, photographs of Ti-doped zirconium oxyfluorides, crystallographic data, and refined atomic parameters (PDF)

■ AUTHOR INFORMATION

Corresponding Author

Yonggang Wang − *Center for High Pressure Science and Technology Advanced Research (HPSTAR), Beijing 100094, China;* orcid.org/0000-0003-4816-9182; Email: yonggang.wang@hpstar.ac.cn

Authors

Chen Li − *Center for High Pressure Science and Technology Advanced Research (HPSTAR), Beijing 100094, China*

Ting Wen − *Center for High Pressure Science and Technology Advanced Research (HPSTAR), Beijing 100094, China;* orcid.org/0000-0001-6572-0920

Ke Liu − *Center for High Pressure Science and Technology Advanced Research (HPSTAR), Beijing 100094, China*

Dequan Jiang − *Center for High Pressure Science and Technology Advanced Research (HPSTAR), Beijing 100094, China;* orcid.org/0000-0003-0998-5507

Zimin Jiang − *Center for High Pressure Science and Technology Advanced Research (HPSTAR), Beijing 100094, China*

Complete contact information is available at: https://pubs.acs.org/10.1021/acs.inorgchem.1c02176

Notes

The authors declare no competing financial interest.

■ ACKNOWLEDGMENTS

This work was supported by the National Natural Science Foundation of China (52073003), Major Program of National Natural Science Foundation of China (22090041), and National Key R&D Program of China (2018YFA0305900).

■ REFERENCES

(1) Aidoudi, F. H.; Aldous, D. W.; Goff, R. J.; Slawin, A. M. Z.; Attfield, J. P.; Morris, R. E.; Lightfoot, P. An ionothermally prepared $S = 1/2$ vanadium oxyfluoride kagome lattice. *Nat. Chem.* **2011**, *3*, 801−806.

(2) Kuriki, R.; Ichibha, T.; Hongo, K.; Lu, D.; Maezono, R.; Kageyama, H.; Ishitani, O.; Oka, K.; Maeda, K. A stable, narrow-gap oxyfluoride photocatalyst for visible-light hydrogen evolution and carbon dioxide reduction. *J. Am. Chem. Soc.* **2018**, *140*, 6648−6655.

(3) Lee, J.; Kitchaev, D. A.; Kwon, D.-H.; Lee, C.-W.; Papp, J. K.; Liu, Y.-S.; Lun, Z.; Clément, R. J.; Shi, T.; McCloskey, B. D.; Guo, J.; Balasubramanian, M.; Ceder, G. Reversible Mn^{2+}/Mn^{4+} double redox in lithium-excess cathode materials. *Nature* **2018**, *556*, 185−190.

(4) Yi, G.; Peng, Y.; Gao, Z. Strong red-emitting near-infrared-to-visible upconversion fluorescent nanoparticles. *Chem. Mater.* **2011**, *23*, 2729−2734.

(5) Mao, F.-F.; Hu, C.-L.; Xu, X.; Yan, D.; Yang, B.-P.; Mao, J.-G. $Bi(IO_3)F_2$: the first metal iodate fluoride with a very strong second harmonic generation effect. *Angew. Chem., Int. Ed.* **2017**, *56*, 2151−2155.

(6) Liang, M.-L.; Hu, C.-L.; Kong, F.; Mao, J.-G. $BiFSeO_3$: an excellent SHG material designed by aliovalent substitution. *J. Am. Chem. Soc.* **2016**, *138*, 9433−9436.

(7) Siao, C.-W.; Lee, W.-L. W.; Dai, Y.-M.; Chung, W.-H.; Hung, J.-T.; Huang, P.-H.; Lin, W.-Y.; Chen, C.-C. $BiO_xCl_y/BiO_mBr_n/BiO_pI_q$/GO quaternary composites: syntheses and application of visible-light-driven photocatalytic activities. *J. Colloid Interface Sci.* **2019**, *544*, 25−36.

(8) Li, M.; Yu, S.; Huang, H.; Li, X.; Feng, Y.; Wang, C.; Wang, Y.; Ma, T.; Guo, L.; Zhang, Y. Unprecedented eighteen-faceted BiOCl with ternary facet junction boosting cascade charge flow and photoredox. *Angew. Chem., Int. Ed.* **2019**, *58*, 9517−9521.

(9) Lin, X.; Huang, T.; Huang, F.; Wang, W.; Shi, J. Photocatalytic activity of a Bi-based oxychloride Bi_3O_4Cl. *J. Phys. Chem. B* **2006**, *110*, 24629−24634.

(10) Huang, H.; Xiao, K.; Du, X.; Zhang, Y. Vertically aligned nanosheets-array-like BiOI homojunction: three-in-One promoting photocatalytic oxidation and reduction abilities. *ACS Sustainable Chem. Eng.* **2017**, *5*, 5253−5264.

(11) Huang, H.; Liu, C.; Ou, H.; Ma, T.; Zhang, Y. Self-sacrifice transformation for fabrication of type-I and type-II heterojunctions in hierarchical $Bi_xO_yI_z$/g-C_3N_4 for efficient visible-light photocatalysis. *Appl. Surf. Sci.* **2019**, *470*, 1101−1110.

(12) Louvain, N.; Karkar, Z.; El-Ghozzi, M.; Bonnet, P.; Guérin, K.; Willmann, P. Fluorination of anatase TiO_2 towards titanium oxyfluoride $TiOF_2$: a novel synthesis approach and proof of the Li-insertion mechanism. *J. Mater. Chem. A* **2014**, *2*, 15308−15315.

(13) Mahenthirarajah, T.; Li, Y.; Lightfoot, P. Hydrothermal synthesis of vanadium oxyfluoride chains incorporating covalently bound copper coordination complexes. *Inorg. Chem.* **2008**, *47*, 9097−9102.

(14) Papiernik, R.; Frit, B. Structure cristalline d'une phase cubique desordonnee de type ReO_3 excedentaire en anions: $ZrF_{2,67}O_{0,67}$. *Mater. Res. Bull.* **1984**, *19*, 509−516.

(15) Flynn, S.; Zhang, C.; Griffith, K. J.; Shen, J.; Wolverton, C.; Dravid, V. P.; Poeppelmeier, K. R. Fluoridation of HfO_2. *Inorg. Chem.* **2021**, *60*, 4463−4474.

(16) Hancock, C. A.; Herranz, T.; Marco, J. F.; Berry, F. J.; Slater, P. R. Low temperature fluorination of $Sr_3Fe_2O_{7-x}$ with polyvinylidine fluoride: An X-ray powder diffraction and Mössbauer spectroscopy study. *J. Solid State Chem.* **2012**, *186*, 195−203.

(17) Hirai, D.; Sawai, O.; Nunoura, T.; Hiroi, Z. Facile synthetic route to transition metal oxyfluorides via reactions between metal oxides and PTFE. *J. Fluorine Chem.* **2018**, *209*, 43−48.

(18) Wang, Y.; Wen, T.; Zhang, H.; Sun, J.; Zhang, M.; Guo, Y.; Luo, W.; Xia, M.; Wang, Y.; Yang, B. Low-temperature fluorination route to Lanthanide-doped monoclinic ScOF host material for tunable and nearly single band up-conversion luminescence. *J. Phys. Chem. C* **2014**, *118*, 10314−10320.

(19) Wen, T.; Zhou, Y.; Yang, B.; Wang, Y. Controllable synthesis, polymorphism and structure-dependent photoluminescence properties of europium oxyfluorides. *Eur. J. Inorg. Chem.* **2017**, 5121−5126.

(20) Wen, T.; Ding, R.; Zhou, Y.; Si, Y.; Yang, B.; Wang, Y. Polymorphism of erbium oxyfluoride: selective synthesis, crystal structure and phase-dependent upconversion luminescence. *Eur. J. Inorg. Chem.* **2017**, 3849−3854.

(21) Joubert, P.; Gaudreau, B. Sur Quelques Oxyfluorures de Zirconium Tétravalent. *Rev. Chim. Miner.* **1975**, *12*, 289−302.

(22) Papiernik, R.; Frit, B.; Gaudreau, B. Les Phases Solides du Système ZrO_2-ZrF_4. *Rev. Chim. Miner.* **1986**, *23*, 400−436.

(23) Gaudreau, B. Recherches Sur le Fluorure de Zirconium et Quelques-Uns de Ses Dérivés. *Rev. Chim. Miner.* **1965**, *2*, 1−52.

(24) Kolditz, L.; Feltz, A. Über fluorhaltige komplexe. III. Über Zirkontetrafluoridhydrate, Zirkonhydroxofluoride und ihre Kondensationsprodukte. *Z. Anorg. Allg. Chem.* **1961**, *310*, 217−224.

(25) Plitzko, C.; Meyer, G. Einkristalle von $(NH_4)ZrF_5$ und $(NH_4)HfF_5$ durch Oxidation von Zirconium und Hafnium mit $(NH_4)HF_2$. *Z. Anorg. Allg. Chem.* **1998**, *624*, 169−170.

(26) Meyer, G. The oxidation of metals with Liebig acids. *Z. Anorg. Allg. Chem.* **2008**, *634*, 201−222.

(27) Hampson, G. C.; Pauling, L. The structure of ammonium heptafluozirconate and potassium heptafluozirconate and the

configuration of the heptafluozirconate group. *J. Am. Chem. Soc.* **1938**, *60*, 2702−2707.
(28) Buslaev, Y. A.; Pachomov, V. I.; Tarasov, V. P.; Zege, V. N. F^{19} spin-lattice relaxation and X-ray study of phase transition in solid K_3ZrF_7 and $(NH_4)_3ZrF_7$. *Phys. Status Solidi B* **1971**, *44*, K13−K15.
(29) Holmberg, B. The crystal structure of $Zr_7O_9F_{10}$. *Acta Crystallogr.* **1970**, *26*, 830−835.
(30) Taylor, D. J.; Meyer, H. M. Wet-chemical synthesis of zirconium oxyfluoride. *J. Mater. Sci.* **2005**, *40*, 2655−2658.
(31) Monnahela, O. S.; Vilakazi, B. M.; Wagener, J. B.; Roodt, A.; Carstens, P. A. B.; Retief, W. L. A thermogravimetric study of the fluorination of zirconium and hafnium oxides with fluorine gas. *J. Fluorine Chem.* **2012**, *135*, 246−249.
(32) Vilakazi, B. M.; Monnahela, O. S.; Wagener, J. B.; Carstens, P. A. B.; Ntsoane, T. A thermogravimetric study of the fluorination of zirconium and hafnium oxides with anhydrous hydrogen fluoride gas. *J. Fluorine Chem.* **2012**, *141*, 64−68.
(33) Laptash, N. M.; Polyshchuk, S. A. Thermal decomposition of ammonium fluoroferrates $(NH_4)_xFeF_{2x}(2\leq x\leq 3)$. *J. Therm. Anal.* **1995**, *44*, 877−883.
(34) Papiernik, R.; Frit, B. Structure cristalline d'une phase semie-ordonnée $ZrF_{3.33}O_{0.33}$. *Ann. Chim.* **1983**, *8*, 509−514.
(35) Papiernik, R.; Mercurio, D.; Frit, B. Structure du tétrafluorure de zirconium, $ZrF_4\alpha$. *Acta Crystallogr.* **1982**, *38*, 2347−2353.
(36) Gualtieri, A.; Norby, P.; Hanson, J.; Hriljac, J. Rietveld refinement using synchrotron X-ray powder diffraction data collected in transmission geometry using an imaging-plate detector: application to standard *m*-ZrO_2. *J. Appl. Crystallogr.* **1996**, *29*, 707−713.
(37) Papiernik, R.; Frit, B. Structure cristalline de la variété basse température de l'oxyfluorure $Zr_3F_8O_2$. *Rev. Chim. Miner.* **1984**, *21*, 321−334.
(38) Legein, C.; Fayon, F.; Martineau, C.; Body, M.; Buzaré, J.-Y.; Massiot, D.; Durand, E.; Tressaud, A.; Demourgues, A.; Péron, O.; Boulard, B. ^{19}F high magnetic field NMR study of β-ZrF_4 and CeF_4: from spectra reconstruction to correlation between fluorine sites and ^{19}F isotropic chemical shifts. *Inorg. Chem.* **2006**, *45*, 10636−10641.
(39) Thompson, J. G.; Withers, R. L.; Kepert, C. J. Incommensurately modulated $ZrO_{2-x}F_{2x}$: $0.698 \leq x \leq 0.714$. *J. Solid State Chem.* **1991**, *95*, 111−125.
(40) Occhiuzzi, M.; Cordischi, D.; Dragone, R. Manganese ions in the monoclinic, tetragonal and cubic phases of zirconia: an XRD and EPR study. *Phys. Chem. Chem. Phys.* **2003**, *5*, 4938−4945.
(41) Laval, J.-P. Crystal chemistry of anion-excess ReO_3-related phases. III. *Acta Crystallogr.* **2014**, *70*, 742−748.
(42) Ishigame, M.; Sakurai, T. Temperature dependence of the Raman spectra of ZrO_2. *J. Am. Ceram. Soc.* **1977**, *60*, 367−369.
(43) Voit, A. V.; Voit, E. I.; Sergienko, V. I. *Ab Initio* study of the structure and vibrational spectra of $ZrFn^{4-n}$ systems. *J. Struct. Chem.* **1999**, *40*, 838−842.
(44) Aimi, A.; Takahashi, H.; Fujimoto, K. Afterglow Properties and Trap-Depth Control in ZrO_2:Ti, *M* ($M = Ca^{2+}$, Y^{3+}, Nb^{5+}, W^{6+}). *Inorg. Chem.* **2020**, *59*, 16865−16871.
(45) Cong, Y.; Li, B.; Lei, B.; Li, W. Long lasting phosphorescent properties of Ti doped ZrO_2. *J. Lumin.* **2007**, *126*, 822−826.
(46) Nakayama, S.; Sakamoto, M. Fluorescence property of ZrO_2:Ti phosphor and its enhancement in fluorescent intensity by adding phosphorus. *J. Mater. Res. Technol.* **2016**, *5*, 289−292.
(47) Sarver, J. F. Preparation and luminescent properties of Ti-activated zirconia. *J. Electrochem. Soc.* **1966**, *113*, 124−128.
(48) Champarnaud-Mesjard, J. C.; Laval, J. P.; Gaudreau, B. Fluorozirconates d'indium et de titane. *Rev. Chim. Miner.* **1974**, *11*, 735−741.
(49) Yang, C.; Zhang, Y.; Bai, J.; Qu, B.; Tong, P.; Wang, M.; Lin, J.; Zhang, R.; Tong, H.; Wu, Y.; Song, W.; Sun, Y. Crossover of thermal expansion from positive to negative by removing the excess fluorines in cubic ReO_3-type $TiZrF_{7-x}$. *J. Mater. Chem. C* **2018**, *6*, 5148−5152.
(50) Lafague-Dit-Hauret, W.; Schira, R.; Latouche, C.; Jobic, S. Theoretical calculations meet experiment to explain the luminescence properties and the presence of defects in *m*-ZrO_2. *Chem. Mater.* **2021**, *33*, 2984−2992.
(51) Wang, Y.; Pan, S. Recent development of metal borate halides: Crystal chemistry and application in second-order NLO materials. *Coord. Chem. Rev.* **2016**, *323*, 15−35.

https://doi.org/10.1021/acs.inorgchem.1c02176
Inorg. Chem. 2021, 60, 14382−14389